Advances in Materials Science and Engineering

WILEY

RESEARCH ARTICLE OPEN ACCESS

Artificial Muscles for Footwear Technology: Knitting Structures With Variable Elasticity

Felipe Sheward[1] | Gaetano Burriesci[1,2,3] | Daniela M. Romano[4]

[1]Department Mechanical Engineering, UCL Cardiovascular Engineering Laboratory, University College London, London WC1E 7JE, UK | [2]Department of Engineering, University of Palermo, Viale Delle Scienze, Edificio 8, Room 1200, Palermo 90128, Italy | [3]Bioengineering & Medical Devices Group, Ri.MED Foundation, Via Bandiera 11, Palermo 90133, Italy | [4]Institute of Artificial Intelligence, De Montfort University, The Gateway, Leicester LE1 9BH, UK

Correspondence: Felipe Sheward (felipe.sheward@ucl.ac.uk)

Received: 5 February 2025 | **Revised:** 11 December 2025 | **Accepted:** 19 December 2025

Academic Editor: Weiwei Kong

Keywords: artificial muscles | compression test | deformation behavior | knitting patterns | metamaterials | shape changing | smart composite | smart footwear | soft robotics | variable stiffness

ABSTRACT

Current commercial midsoles provide a fixed level of cushioning and elasticity regardless of gait phase or loading rate. We report a novel "artificial muscle" midsole composite that dynamically tunes its compressive stiffness and relaxation behavior by embedding nickel–titanium (Nitinol) shape-memory alloy (SMA) wires into multilayer silicone substrates (Shore A12, A20, A30) using two hand-knitting patterns (A and C). Specimens (undeformed height = 30 mm; frontal area = 61,213.856 mm^2 or 612.139 cm^2) were tested on a 50 kN Instron 5969 under displacement control. For compression (stress–strain) testing, each sample was ramped from an initial grip separation of 30 mm to a 12.5 mm gap (≈58.33% nominal compressive strain) at 200 mm/min (≈0.111 s^{-1} strain rate). At each voltage state (0 V ⟶ 14 V for Pattern A; 0 V ⟶ 10 V for Pattern C), four loading–unloading cycles were conducted at 60 mm/min (≈0.033 s^{-1} strain rate). For stress-relaxation (creep) testing, specimens were ramped from 30 mm to a 12.5 mm gap (≈58.33% strain) at 60 mm/min (≈0.033 s^{-1}) and then held at constant displacement for 120 s under three voltage levels (Pattern A: 0 V, 14 V, 19 V; Pattern C: 0 V, 8 V, 14 V). Under these protocols, silicone A30 with Pattern C consistently exhibited the largest actuation-induced contraction ($\Delta = 27.79\%$ in compression; $\Delta = 36.54\%$ in creep/relax), while MANOVA and *t*-test results confirmed that substrate hardness, actuation state, and knitting pattern each significantly modulated compressive stress (all $p < 0.001$). These findings demonstrate that our SMA-enabled midsole can switch between soft and stiff modes—across ≈58.3% strain at strain rates up to ≈0.111 s^{-1}—offering a tunable, durable, and cost-effective solution for adaptive footwear.

1 | Introduction

Footwear has an essential role in our well-being, reducing the risk of falls, enhancing cushioning, and decreasing pain and impairment [1, 2]; constraints during walk also affect how we interact; for example, most falls occur as we move rather than standing [3], while responses to disturbances in the standing phase follow a short–medium–long latency response pattern over 50–200 ms, in muscular activation while walking can occur at any time over a period much more extended (600 ms); in this sense, the body configurations change dramatically during the gait cycle, requiring different mechanisms to maintain the upright balance at different points of the cycle [4, 5].

Studies have found that maximalist shoes may reduce the pronation component in tibial stress fractures (TSFs) in female runners, reducing the peak ankle eversion and ankle internal rotation (ROM), in comparison with neutral shoes, also

a decrease in the ankle internal rotation in flexible shoes compared with neutral footwear [6]. TSFs are frequent and serious injuries in runners, especially in females [7]. Cushioned shoes are better at reducing tibial acceleration and tibial shock, and stability shoes can reduce rearfoot eversion and eversion excursion [8]. Longitudinal bending stiffness varies depending on the running speed; this may affect and produce changes in horizontal ground reaction forces, spatiotemporal variables, subjective comfort, and metabolic cost. In this sense, an optimal bending stiffness can reduce metabolic cost and improve comfort but it may be dependent on the running speed [9].

The running shoe is a net dissipator of energy; the exchanges of it depend on the cushioning material properties and the runner's plantar pressure distribution and how the energy storage and recovery occur throughout the step in different regions of the shoe midsole [10]. Other factors that affect the energy when running are the environmental temperatures on the midsole; results show that when increasing the temperature, the peak deceleration and energy absorption decreased; however, the times to peak deceleration and peak deformation increased, suggesting that in cold environments, they will contribute to an insufficient cushioning and in hot environments they will provide an inadequate rearfoot control [11].

The cushioning characteristics of sport shoes change with increasing mileage; studies show an increase in peak force after 500 km, which is consistent with machine-simulated studies of cushioning deterioration [12]. Running footwear are made of different materials, particularly in the sole region, where the rigidity significantly impacts movement mechanics. For example, while the hardness of the shoe sole does not affect the initial peak force or knee joint motion, it does influence the timing and rate of force application, as well as specific movements of the ankle joint, particularly in softer composites [13].

Muscle control also provides additional support to the foot and compensates for any inadequate gait patterns [14], but there are limits to the capacity of muscular compensations; for example, in army recruits with low-arched feet, fatigue of the controlling muscles was suggested as a factor fracture and pain during training exercises [15–17]. At the same time, studies on fatigue and postural compensation, using ankle destabilization devices, try to uncover the causes of how muscle activation can compensate for walking deficiencies [18, 19], or the influence of reduced plantar sensation on pressure distribution by applying an ice immersion approach in barefoot walking [20, 21], which are commonly studied in research.

In this sense, an important area of discussion in muscle control is modifications in longitudinal bending stiffness, also called LBS, which has gained relevance in understanding the role of footwear in movement [22, 23]. Also, in forefoot bending stiffness reduces injury, decreasing the amount of metatarsophalangeal extension (MTP) [23–25], especially in athletes [26, 27], running performance [28, 29], jumping [30], and also as a treatment for metatarsal stress using military boots [31]. When looking for materials with the ability to modify their stiffness, we can identify several areas of development of smarter materials with tunable properties that could be applied in footwear technology to improve performance in movement and support muscle control. For example, advances in additive manufacturing techniques offer researchers the ability to modify the internal structures in 3D cell arrangements, providing thousands of degrees of freedom for the development of smarter systems with multifunctional capabilities, otherwise known as metamaterials [32, 33]. Examples can be found in several areas, for instance, in the footwear industry using hyperplastic foams [34], in foot deformation in sole design to personalize the deformation behavior [35], in foot orthoses in patients with diabetes mellitus [36], or using piezoelectric to harvester energy from during walk [37]. In this sense, 3D printing has opened new opportunities for the development of smart materials, for example, by converting the mechanical properties of hard materials [38], designing the internal structure of objects by introducing hollowing optimization in honeycomb-cell structures [39, 40], or by modifying the volume and the balance of internal configurations [41] has enabled the fabrication of complex geometries in metamaterials, allowing elaborate behaviors and physical properties [42], such as in origami-based designs with several areas of applications, for example, self-folding systems [43, 44], mechanical metamaterials [45, 46], or medical stents using shape memory alloys (SMAs) [47]; here, the SMA adds multifunctional qualities to the structure, either by its shape memory effect [48] or due to its biocompatibility [49, 50].

An actuator capable of producing changes in its structure is artificial muscles, which are a series of connected microactuators that form a larger one [51], where recent advances in nanomaterial fabrication and characterization have resurfaced the development of this type of soft robotics [52]. Here, the term artificial muscle refers to a class of material capable of reversibly contracting, expanding, or rotating within one component from a stimulus (voltage, current, pressure, temperature, light, among others), allowing to produce other types of motion if combined, such as bending or more complex types of actuations that are compressing one side and releasing in another part [53].

An important field transforming reversibly between the two phases is SMAs, allowing the development of new and smarter actuators in several areas; for instance, in materials and composites with stiffness variations; for example, changes in bending stiffness in footwear have been demonstrated to improve performance in movement and reduce injury by modifying the center of pressure, especially in sports [54, 55]. Here, the biomechanics of movement plays a significant role in the development of assistive technology with muscle actuation. For instance, during walk, the knee is one of the parts of the body that needs support, especially when it has weakened because of an injury, age, or weight, among others; they are some novel assistive knee brace with wire actuators made of SMAs; this mechanism can improve the weight and flexibility issues [56], also in the development of small SMA biped robot to improve stability during locomotion [57, 58], or in ankle foot orthoses developed with SMA capable of producing mechanical stiffness variations that emulate a healthy muscle capable of reducing the metabolic energy during walk that depends on the angle of the joint to enhance mobility, and the duration of activities can be longer prior to fatigue [59].

When examining variable stiffness research in footwear technology, it is possible to find several examples in prosthetics, for example, in the development of a prosthetic foot capable of changing the stiffness up to 50% in the sagittal plane to improve mobility in multiple terrain conditions [60], using custom 3D-printed footwear to reduce stress distribution [61], utilizing pneumatic actuation by developing an interactive shoe using air pressure to change the inflation within a sole to alter users gait in soft robotics [62],

developing faster pneumatic networks (pneu-net) actuation [63], or by controlling lower limb muscle activity during walk, using an insole-embedded actuator to alter the shape and hardness of the footwear influencing muscle activity [64].

Overall, the literature highlights the growing importance of footwear technologies capable of adapting their mechanical properties to user-centric demands. Despite notable advances in the control of cushioning materials, all current footwear solutions rely on passive or semi-passive structures with limited capacity of real-time adaptability. The integration of smart materials such as SMAs and tunable composites offers an opportunity to bridge this gap, enabling the footwear system to actively respond to changes in load, temperature, and motion. However, few studies have explored the combination of soft elastomeric substrates with active actuation mechanisms to achieve controlled stiffness modulation. This study addresses these limitations by developing a new class of adaptive artificial muscles for footwear applications, capable of modulating their stiffness and stress distribution in response to changes in temperature.

2 | Method

2.1 | Mechanical Testing or Characterization

We developed a support structure that we can test several knitting techniques, allowing us to obtain different actuation results depending on the knitting pattern used, which shows to be a more straightforward technique to embed. To test it, we developed an open linear configuration in opposite directions using a tubing technique to channel the SMA wire, adding different layers of flexibility control as a series of artificial fibers that can affect the construction cell. By investigating the actuation of each cell of the footwear independently allowed us to further miniaturize the model and embed more SMA per cubic centimeter.

This research focuses on developing and understanding the use of innovative embedding techniques, specifically called knitting patterns, as they are hand-knitted into a support structure to enhance the performance of a soft actuator (artificial muscle) integrated into a midsole structure for footwear technology.

The goal is to investigate the influence of different silicone shore hardness levels (A12, A20, A30) on the mechanical properties of these artificial muscles, particularly their stress performance during compression. We seek to identify the most effective methods for embedding SMAs into silicone substrates to improve stress handling and overall performance.

By examining various knitting patterns, we aim to determine the optimal configurations for embedding Nitinol wire, achieving variable hardness and improved elasticity in the midsole. Additionally, the research will explore the compression properties of the midsole, the cyclic loading and unloading behaviors, and the functional performance in terms of movement efficiency, energy return, shock absorption, comfort, and injury prevention. The interaction effects between material type, actuation status, and knitting pattern will be analyzed to identify optimal performance combinations. Comparative analysis will be conducted to evaluate the smart midsole against traditional midsoles and other adaptive footwear technologies. The study also includes creep and relaxation tests to assess the long-term compression behavior and statistical analysis to determine significant differences in performance across materials and knitting patterns. Ultimately, our objective is to advance the development of smart, adaptive materials in footwear technology, providing novel insights into the interaction between Nitinol wire and silicone support structures and pushing the boundaries of current knowledge in smart footwear materials.

3 | Embedding Technique

3.1 | Knitting Patterns

We developed a series of embedding techniques in serval silicone substrates of different shores (A12/A20/A30) that we called knitting patterns, because we hand-knit each substrate and analyzed its elastic behavior. We measured the amount of contraction (artificial muscle behavior) while applying temperature to the SMA (Flexinol SMA) embedded in a silicon prototype. Flexinol is an SMA made of nickel titanium capable of contracting 2%–5% of its length [65, 66], developed by FLEXINOL® and Muscle Wires®, which are Registered Trademarks of DYNALLOY, Inc. Copyright©2024 DYNALLOY, Inc. (see Table 1).

During the embedding, the SMA is knitted in the substrate back and forth along a row through a series of adjacent tubing in a path, described in a series of patterns tested in a tensile and compression manner.

3.1.1 | Knitting Pattern A

The SMA wire is knitted in a back-and-forth pattern along a first row in a first direction and then in a back-and-forth pattern along a second row in a second direction, opposite the first direction; see Figure 1.

3.1.2 | Knitting Pattern C

The SMA wire is knitted in a back-and-forth pattern along a first row in a first direction to the mid-point of the substrate and then in a back-and-forth pattern along a second row in a second direction, opposite the first direction. A second SMA wire is knitted in a back-and-forth pattern from the second edge in a first direction to the mid-point of the substrate and then in a back-and-forth pattern along a second row in a second direction, opposite the first direction; see Figure 2.

3.2 | Test Sample

For the development of a composite capable of dynamically changing its flexibility, we started by exploring the literature on objects with multiple cells to control elasticity.

Particularly, we observed the embedding techniques, especially the use of fibers to produce tensile actuation and control expanding deformation in artificial muscles. Through this, we started developing a series of prototypes using arrays of fibers to channelize the SMAs when embedded on a series of interconnected tubing to maximize the contraction when actuated.

To build the prototype for testing, we subdivided the midsole area of the footwear into eight parts: the right and left hemispheres of the heel and midfoot and four parts on the forefoot. We concentrated on section A (heel) of the picture below to conduct our test; see Figure 3.

The samples tested for the compression test were assessed using a specimen of volumetric mesh consisting of a series of multilayer silicone tubes alternating at +45° and −45°. Tubes had an external

TABLE 1 | Flexinol actuator wire technical sheet.

Diameter size inches (mm)	Resistance ohms/inch (ohms/meter)	Heating pull force pounds (grams)	Cooling deformation force pounds (grams)	Approximate current for 1 s contraction (mA)	Cooling time 158°F, 70°C "LT" wire (seconds)	Cooling time 194°F, 90°C "HT" wire (seconds)
0.020 (0.51)	0.11 (4.3)	7.85 (3560)	3.14 (1424)	4000	16.8	14.0

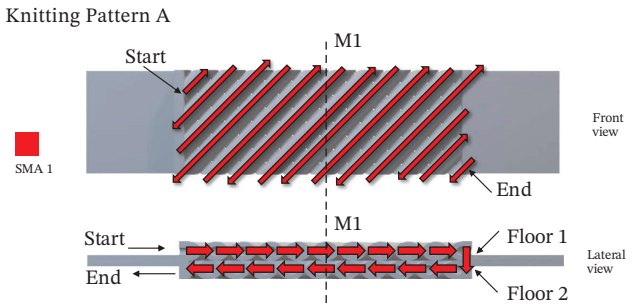

FIGURE 1 | Knitting Pattern A.

diameter of 4 mm, a wall thickness of 1.2 mm, and a distance between the axes of two adjacent tubes in each layer equal to 6 mm; see Figure 3. To control the suspension in the metamaterial, we used a system of inner tubing of 1.4 mm diameter to reinforce the connections between the six layers and an area of 61,213.856 mm^2 (612.139 cm^2). The substrate was 3D-printed using an Ultimaker S3 with an Ultimaker PVA (polyvinyl alcohol) Filament Natural, which is a water-soluble support material for multiextrusion 3D printing, using the software Cura 5.3.0. The prototypes were developed and tested using Solidworks 2023, and the PVA casting mold was built on Autodesk Fusion 360. After dissolving the PVA, 0.51 mm-diameter Flexinol® Nitinol wires were hand-knitted through adjacent tubes according to Pattern A or Pattern C, creating a uniform "artificial muscle" network.

The silicone-based substrate was specifically engineered to maximize contractile behavior by embedding SMA wires within a controlled, multicell metamaterial network. A tubing network was generated to test and investigate the effects of different SMA-embedding techniques in medium-hard silicone composites. This interconnected tubing network forces all cells to deform uniformly; changing tube geometry (diameter, wall thickness, interlayer spacing) or rerouting SMA wires (knitting pattern) directly affects how compressive stresses distribute and relax. The multicell design not only allows direct comparison of the two embedding techniques but also enables tailoring of midsole stiffness over a broad range (up to ≈58% compressive strain) by manipulating tube geometry and interlayer spacing.

Variations in the internal tube diameter, wall thickness, and knitting layout directly impact force distribution and stress-relaxation behavior—key factors in achieving improved weight distribution and balance compared to conventional running shoe midsoles; see Figure 4.

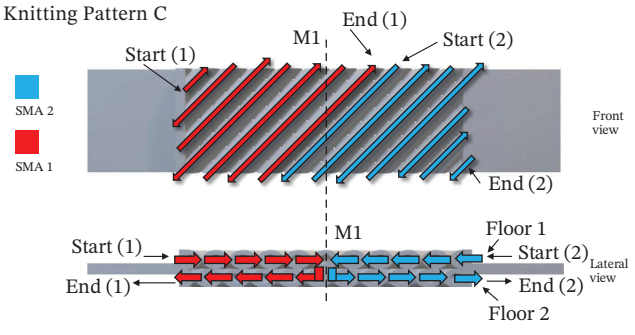

FIGURE 2 | Knitting Pattern C.

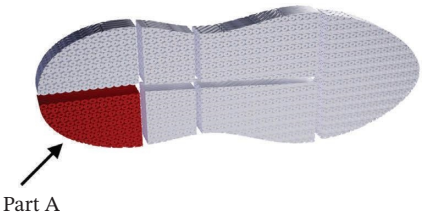

FIGURE 3 | Section A of the footwear tested on all compression tests.

This design allows the material to exhibit controlled elasticity and flexibility, which can be dynamically adjusted based on the specific requirements of the application. The support structure enables the customization of the composite material for different applications. By varying the design, the researchers can tailor the mechanical properties of the material to meet specific needs. This versatility is particularly important in applications like soft robotics and wearable devices, where different levels of stiffness and flexibility may be required.

4 | Mechanical Testing Footwear

Tests were performed on a 50 kN Instron 5969 using the software Bluehill Universal version 4.06 to test the stress–strain also using a creep and relax to further explore the stability of each sample at the Materials Laboratory at University College London in Mechanical Engineering, Roberts Engineering Building, University College London, Torrington Place, London WC1E 7JE.

4.1 | Compression Displacement

During stress–strain compression displacement, we run a displacement control test of the specimen applying 4 cycles on each voltage (0 V–14 V) for knitting Pattern A, and (0 V–10 V) for knitting Pattern C, setting a displacement of 30 mm (grip-to-grip separation at start position), point of load application of the circles of 12.5 mm with a speed at the start point of 200 mm/min, and a speed of cycles of 60 mm/min; see Figure 5.

4.1.1 | Test Method

This is a displacement control test, meaning that the amount of displacement (movement) applied to the specimen is controlled, rather than the force.

4.1.2 | Voltage Ranges

The test involves varying the voltage applied to the knitting patterns:

- For knitting Pattern A, the voltage is applied in the range of 0 V–14 V.
- For knitting Pattern C, the voltage range is 0 V–10 V.

4.1.3 | Cycles

For each voltage level, 4 cycles are applied to the specimen. A cycle in this context means repeating the same loading and unloading (compression and release) processes.

4.1.4 | Displacement Setup

The displacement (distance between grips) at the start of the test is set to 30 mm. This is the distance between the grips holding the specimen.

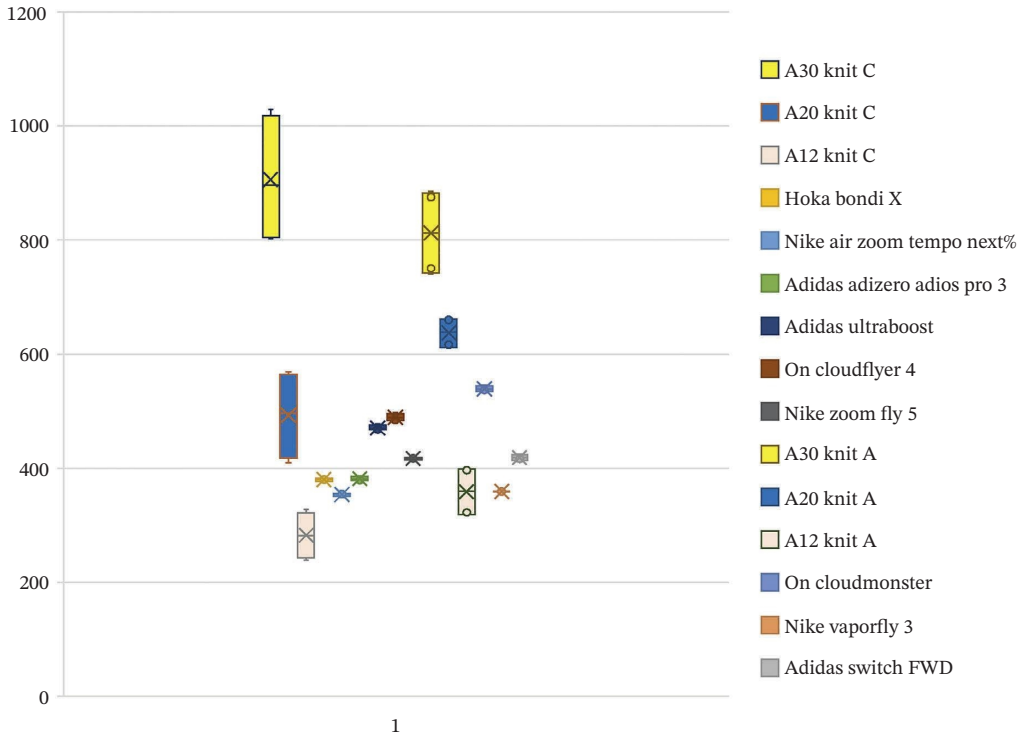

FIGURE 4 | Footwear heel compression test comparison between all market footwears and silicone prototypes using the knitting patterns in Newton (N).

4.1.5 | Point of Load Application

The area where the load is applied is described as having circles with a 12.5 mm diameter.

4.1.6 | Speed at Start Point (200 mm/min)

The test begins with the grips moving apart at a speed of 200 mm per minute.

4.1.7 | Cycle Speed (60 mm/min)

During the cyclic loading part of the test, where the material is repeatedly stretched, the grips move at a slower speed of 60 mm per minute.

This procedure is used to evaluate the behavior of the material (knitting Patterns A and C) under controlled compression, while measuring the stress–strain response at different voltages. The cyclic nature of the test indicates that the material's performance over multiple compressions is being studied.

4.2 | Creep and Relaxation Test

Creep and relax was tested at a displacement of 12.54 mm for 120 s at different voltages (0 V, 14 V, 19 V) for knitting Pattern A and voltages (0 V, 8 V, 14 V) for Pattern C using the same specimens of the compression test; see Figure 5. Creep refers to the tendency of a material to deform gradually under constant stress over time, and

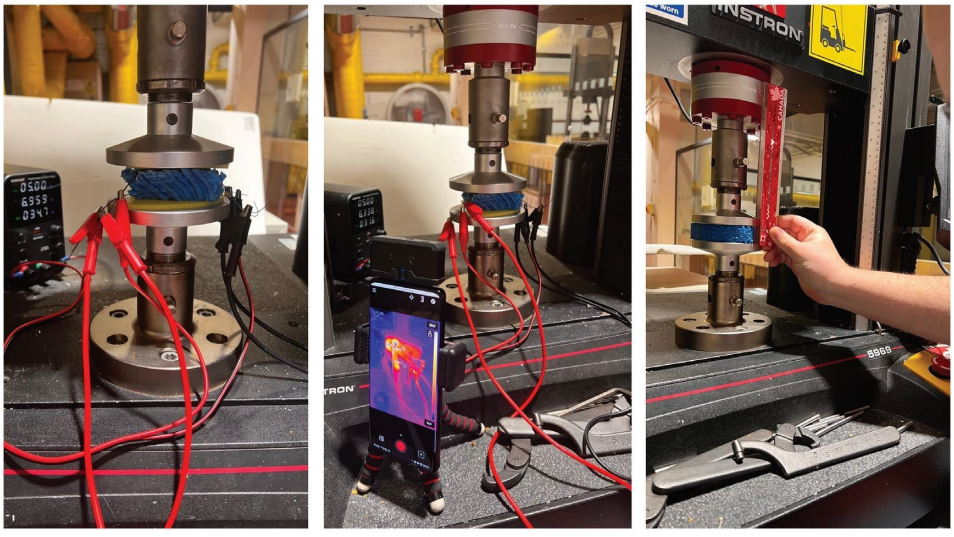

FIGURE 5 | Stress–strain compression displacement.

relaxation refers to the reduction in stress over time while the material is held at a constant strain (displacement in this case).

4.2.1 | Displacement Setup

In this test, the specimen is displaced (compressed) by 12.54 mm. This displacement is maintained for a period of 120 s.

4.2.2 | Voltage Ranges

- For knitting Pattern A, the test is conducted at voltages of 0 V, 14 V, and 19 V.
- For knitting Pattern C, the test uses voltages of 0 V, 8 V, and 14 V.

These different voltage levels are used to investigate the behavior of the material under varying electrical stimulation, as voltage actuates the SMA affecting the material's mechanical properties in this context.

4.2.3 | Test Duration

The displacement is held for 120 s to allow the material to exhibit its creep or relaxation characteristics. Over this period, the material may continue to deform (creep) or experience stress relaxation.

4.2.4 | Specimens

The specimens used for this creep and relaxation test are the same as those used in the compression test.

This test aims to examine how the material (with knitting patterns A and C) behaves when held under constant displacement for an extended period at different voltage levels, focusing on how the material continues to deform (creep) or reduce stress (relax) over time.

This procedure is used to evaluate the behavior of the material (knitting patterns A and C) under controlled compression while measuring the stress–strain response at different voltages. The cyclic nature of the test indicates that the material's performance over multiple compressions is being studied. On the other hand, the creep and relax test aims to examine how the material (with knitting patterns A and C) behaves when held under constant displacement for an extended period at different voltage levels, focusing on how the material continues to deform (creep) or reduce stress (relax) over time; see Figure 5.

4.3 | Data Analysis and Statistical Methods

All results were analyzed using SPSS statistics, Python's Spyder IDE 5.5.1 (conda), and Microsoft Excel. Data were analyzed for statistical significance by multivariate analysis of variance (MANOVA) for the compression test and an independent *t*-test for the creep and relax test. $p < 0.05$ was considered statistically significant.

5 | Results

5.1 | Compression Strength of Silicone Substrates

The results of the compression A12, A20, and A30 at different voltage/temperatures (0 V, 14 V) for knitting Pattern A and voltages (0 V, 10 V) for Pattern C are shown in Figure 6.

Results from the compression test show that when using silicone shore A12 with knitting Pattern A, the compressive stress of the material without voltage (OFF) was 0.0052 MPa, and when 14 V was applied (ON), the stress increased to 0.0065 MPa. This produced a maximum difference of 0.0013 MPa, representing a 20.44% increase in stress between the ON and OFF conditions. In comparison, knitting Pattern C with the same material (A12) exhibited a greater stress increase. Without voltage (OFF), the compressive stress reached 0.0039 MPa, and when 14 V was applied (ON), the stress rose to 0.0054 MPa. This resulted in a maximum difference of 0.0014 MPa, which represents a 26.99% increase in stress, higher than that of knitting Pattern A (see Figure 6).

Data show that knitting Pattern C is a softer composite under both temperature treatments, but it also produces the highest contraction difference between the two, which corresponds to a 26.99% increase, suggesting that knit C allows for greater contraction under compressive forces compared to knit A. The higher percentage difference between the minimum and maximum stresses for knit C indicates that this pattern may be better suited for applications requiring greater adaptability and responsiveness to mechanical deformation.

On the other hand, results from the compression test show that when using silicone shore A20 with knitting Pattern A, the compressive stress of the material without voltage (OFF) was 0.00998 MPa, and when 14 V was applied (ON), the stress increased to 0.01082 MPa. This produced a maximum difference of 0.00084 MPa, representing a 7.83% increase in stress between the ON and OFF conditions (see Figure 6). In comparison, knitting Pattern C with the same material (A20) exhibited a greater stress increase. Without voltage (OFF), the compressive stress reached 0.00671 MPa, and when 14 V was applied (ON), the stress rose to 0.00929 MPa. This resulted in a maximum difference of 0.00258 MPa, which represents a 27.79% increase in stress, higher than that of knitting Pattern A.

This suggests that Pattern C showed not only a higher absolute stress under both conditions but also a significantly larger difference, indicating superior enhancement in stress performance due to voltage application compared to Pattern A.

Finally, results from the compression test show that when using silicone shore A30 with knitting Pattern A, the compressive stress of the material without voltage (OFF) was 0.01209 MPa, and when 14 V was applied (ON), the stress increased to 0.01447 MPa. This produced a maximum difference of 0.00238 MPa, representing a 16.40% increase in stress between the ON and OFF conditions, while the knitting Pattern C with the same material (A30) exhibited a greater stress increase. Without voltage (OFF), the compressive stress reached 0.01312 MPa, and when 14 V was applied (ON), the stress rose to 0.01682 MPa. This resulted in a maximum difference of 0.00369 MPa, which represents a 21.96% increase in stress, higher than that of knitting Pattern A (see Figure 6).

This suggests that the A30 substrate with Pattern C achieved the highest stress values and the largest difference between ON and OFF states among all tested combinations, highlighting its exceptional capability to withstand compressive stress under electrical actuation on higher shore silicones.

The data in Figure 7 reveal a comparison of the compressive stress differences across various combinations of materials and knitting patterns.

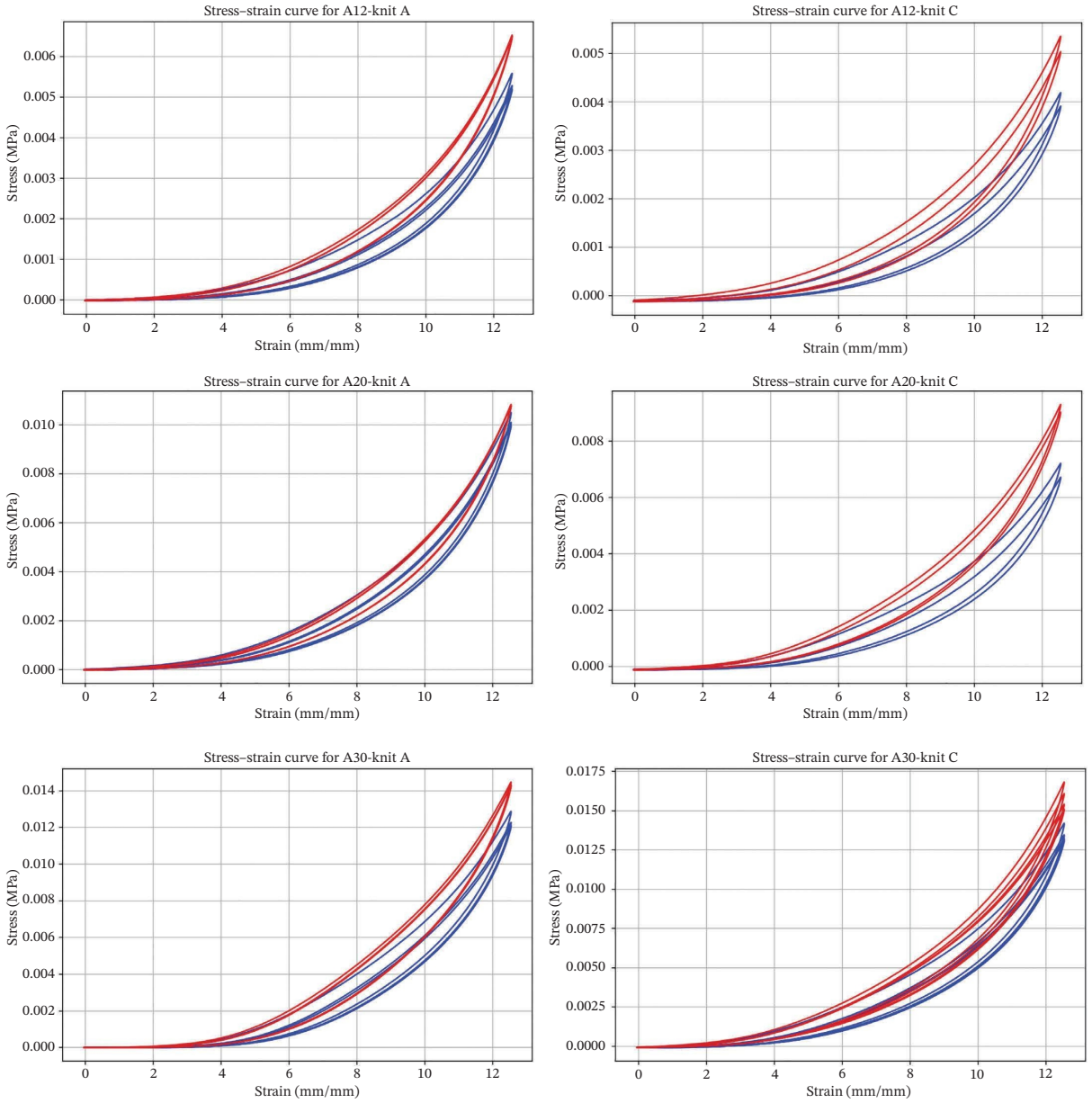

FIGURE 6 | Compressive stress (MPa) versus compressive strain (mm/mm) plot, where the blue lines represent the material without voltage (OFF) and the red lines represent the material with voltage (ON).

The results from the compression test provide valuable insights into the mechanical behavior of different silicone shore materials (A12, A20, A30) and their associated knit patterns (knit A and knit C) under compressive forces (see Figure 7).

Across all materials, knit C consistently exhibited a higher percentage increase in compressive stress between minimum and maximum values compared to knit A. This suggests that knit C allows for greater deformation under compressive loads, making it a more adaptable structure in applications where flexibility and stress variability are important.

Material A12, knit C demonstrated a 26.99% increase in compressive stress, compared to knit A 20.44% increase. The difference in stress values between the two knit patterns highlights that knit C enables the material to better respond to compressive forces. In contrast, knit A, with its relatively lower percentage increase, suggests a more rigid response, providing greater stability under load but less adaptability.

The behavior of Material A20 further reinforces this trend, with knit C showing a 27.79% increase in stress, significantly higher than knit A of 7.83%. The large disparity between the two knit types in this material suggests that knit C offers significantly more flexibility, making it a superior choice in contexts requiring the material to absorb more strain without failure. Conversely, the narrow stress variation in knit A may be advantageous in applications requiring consistent, predictable material performance under compression.

For Material A30, the findings similarly highlight the adaptability of knit C, with a 21.96% increase in stress, compared to 16.40% for knit A. While the percentage difference is smaller than in Materials A12 and A20, the trend remains consistent,

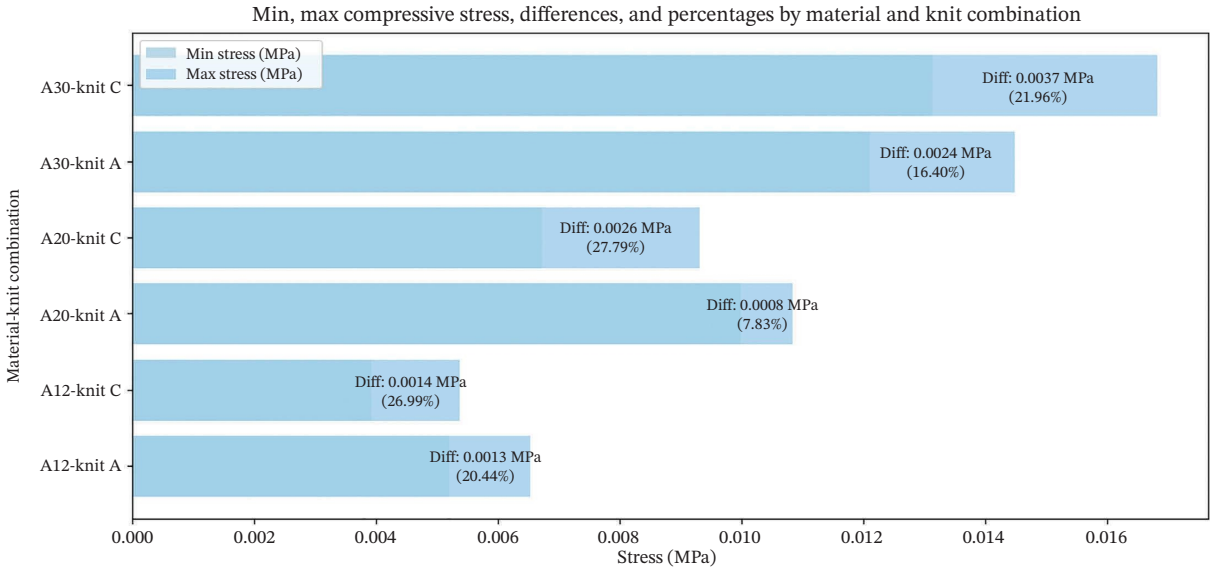

FIGURE 7 | All substrate (A12, A20, and A30) differences between ON and OFF among the cycles and their percentage of difference.

indicating that knit C generally promotes a more flexible material response, while knit A supports a more stable, rigid structure.

The compression tests conducted on Materials A12, A20, and A30 with different knit patterns have revealed important differences in mechanical performance. Knit C, across all materials, allows for greater stress variation, indicating higher flexibility and adaptability under compressive forces.

These findings underscore the importance of selecting the appropriate knit pattern based on the specific performance requirements of the material in real-world applications. For applications requiring greater flexibility and stress absorption, knit C is likely the superior option, while knit A is more suited for scenarios where rigidity and stability are paramount.

5.1.1 | Implications

- Knitting pattern preference: Based on the results, knitting Pattern C is generally more effective in improving stress performance under electrical actuation for all tested substrates. This makes it a preferable choice for applications requiring enhanced stress resistance.
- Substrate choice: The choice of substrate (A12, A20, A30) should be guided by the specific stress requirements of the application. For example, A30 with Pattern C offers the highest stress resistance and might be suitable for applications demanding maximum durability and strength.

The results indicate that knitting Pattern C, particularly when used with the A30 substrate, provides the best performance in terms of stress response to electrical actuation. This finding can guide the development and optimization of materials for applications requiring precise and adaptable stress management.

5.2 | Statistical Analysis

A MANOVA was performed to examine the effects of material used on the samples (A12, A20, and A30), the knitting patterns (A, C), and whether the composite was actuated or not (ON, OFF) on the dependent variables: time, displacement, force, strain, and stress.

The MANOVA results showed significant effects for the material (F (10.000, 417036.000) = 3331.963, $p < 0.001$, partial eta-squared = 0.074, indicating approximately 7.4% of the variance), ON/OFF (F (5.000, 208517.000) = 8625.693, $p < 0.001$, partial eta-squared = 0.171 indicating approximately 17.1% of the variance), knit (F (5.000, 208517.000) = 1879.241, $p < 0.001$, partial eta-squared = 0.043 indicating approximately 4.3% of the variance). Significant interactions were found between the material and ON/OFF (F (10.000, 417036.000) = 1599.936, $p < 0.001$, partial eta-squared = 0.037 indicating approximately 3.7% of the variance), material and knit (F (10.000, 417036.000) = 330.075, $p < 0.001$, partial eta-squared = 0.008 indicating approximately 0.8% of the variance), ON/OFF and knit (F (5.000, 208517.000) = 456.331, $p < 0.001$, partial eta-squared = 0.011 indicating approximately 1.1% of the variance), and a three-way interaction between the material, ON/OFF, and knit (F (10.000, 417036.000) = 222.375, $p < 0.001$, partial eta-squared = 0.005 indicating approximately 0.5% of the variance). Results showed that the interaction effects between the dependent variables had a smaller effect size compared to the main effects, which is visible in the partial eta-squared (n^2). This allowed us to confirm that the material, ON/OFF, and knit explain a large portion of the variance in the dependent variables compared to the interaction effects, suggesting that individual factors influence the outcomes more than their combined interactions.

5.2.1 | Main Effects

- Material: The significant main effect for material (F (10.000, 417036.000) = 3331.963, $p < 0.001$, partial eta-squared = 0.074). This suggests that the type of silicone substrate (A12, A20, A30) plays a crucial role in determining the dependent variables (time, displacement, force, strain, and stress). Approximately 7.4% of the variance in these variables can be attributed to the material used, indicating a substantial influence.

- ON/OFF status: The significant main effect for ON/OFF status ONOFF (F (5.000, 208517.000) = 8625.693, $p < 0.001$, partial eta-squared = 0.171). This indicates that whether the composite is actuated or not has a significant impact on the performance, accounting for about 17.1% of the variance. This large effect size suggests that actuation greatly enhances or alters the material properties under compression.
- Knitting pattern: The significant main effect for knitting pattern knit (F (5.000, 208517.000) = 1879.241, $p < 0.001$, partial eta-squared = 0.043). This shows that the pattern (A or C) used also significantly affects the performance, with about 4.3% of the variance explained by this factor.

5.2.2 | Interaction Effect

- Material and ON/OFF: The interaction between material and actuation status (F (10.000, 417036.000) = 1599.936, $p < 0.001$, partial eta-squared = 0.037), which indicates that the effect of actuation on the dependent variables varies depending on the material type. This interaction accounts for approximately 3.7% of the variance, suggesting a moderate but significant combined effect.
- Material and knit: The interaction between material and knitting pattern knit (F (10.000, 417036.000) = 330.075, $p < 0.001$, partial eta-squared = 0.008) explains about 0.8% of the variance, indicating that the effectiveness of different knitting patterns varies with the type of silicone substrate.
- ON/OFF and knit: The interaction between actuation status and knitting pattern (F (5.000, 208517.000) = 456.331, $p < 0.001$, partial eta-squared = 0.011) shows that the impact of actuation on the dependent variables is influenced by the knitting pattern used, accounting for approximately 1.1% of the variance.
- Three-way interaction: The three-way interaction among material, ON/OFF status, and knitting pattern (F (10.000, 417036.000) = 222.375, $p < 0.001$, partial eta squared = 0.005) explains about 0.5% of the variance, suggesting that while the interaction is significant, it has a smaller effect size compared to the main effects.

Levene's test of equality of error variance indicates that the assumption of homogeneity of variances was violated for all dependent variables; time F (11, 208521) = 17403.571, $p < 0.001$, displacement F (11, 208521) = 4238.621, $p < 0.001$, force F (11, 208521) = 4117.784, $p < 0.001$, strain F (11, 208521) = 4238.527, $p < 0.001$, and stress F (11, 208521) = 4117.777, $p < 0.001$. Results from Levene's test indicate that the variance of the dependent variables is not equal across groups (material, ON/OFF, and knit). On the other hand, the between-subject effects showed significant influence of the main factors and their interactions on the dependent variables. This indicates that the material, ON/OFF, and knitting pattern used significantly influenced the dependent variables individually and through their interactions, where the effect sizes suggest that ON/OFF had a stronger influence on time, while the other variables had smaller but also significant variance.

Post hoc multiple comparisons: Tukey HSD and Bonferroni tests for the dependent variables across their different silicone materials (A12, A20, and A30) showed significant mean differences for all variables $p < 0.001$ with a 95% confidence interval (CI) that does not include zero, confirming the material differences for each dependent variable (time, displacement, force, strain, and stress).

5.2.3 | Implications

These results have several practical implications:

- Material selection: A30 substrate shows a larger variance and higher stress levels, indicating it may be suitable for applications requiring higher stress tolerance but with a trade-off in predictability.
- Knitting pattern: The choice of knitting pattern significantly affects material performance, suggesting that optimizing the pattern could tailor material properties for specific applications.

Overall, the study underscores the importance of considering material composition, actuation status, and knitting pattern in designing and utilizing silicone-based composites for various engineering applications.

5.3 | Creep and Relax

The results of the creep and relax test using the substrates A20 and A30 at different voltage/temperatures (0 V, 14 V and 19 V) for knitting Pattern A and voltages (0 V, 8 V and 14 V) for Pattern C are shown in Figure 8.

Results from the creep and relax test compressive on the substrate A20 with the knitting Pattern A, at 0 V (OFF), a stress of 0.0079 MPa and 0.0092 MPa when actuates (ON), which represent a difference of 0.0013 MPa, which represents a 16.46% percentage change in stress. On the other hand, when using the substrate A20 but now with the knitting Pattern C, it showed a stress of 0.0052 MPa at 0 V and 0.0071 MPa when actuated (ON), exhibiting a higher difference of 0.0019 MPa, representing an increase in stress of 36.54%, the highest among all tests; see Figure 8.

When inspecting the creep and relax test using the A20 substrate in both knitting patterns (Figure 8), again, knitting Pattern C was the softest sample but the highest performer when comparing the difference between OFF and ON. When observing the figure, it is possible to observe the difference in MPa. The analysis indicates that the substrate material and knitting pattern both play crucial roles in determining the stress behavior of the material under actuation. Substrate A20 with knitting Pattern C exhibits the highest stress increment and percentage growth when actuated, suggesting that it may be the most responsive combination among those tested.

When analyzing the following substrate A30 using the knitting Pattern A, it is possible to observe that it reaches a stress of 0.0093 MPa at 0 V and a stress of 0.0122 MPa when actuated, which represent a difference between ON and OFF of 0.0029 MPa, which again is increased when using the knitting Pattern C that achieves 0.0098 MPa when OFF and 0.0133 MPa when actuated, representing a difference of 0.0035 MPa; see Figure 9.

Figure 9 shows that on the creep and relax test using the A30 silicone, knitting Pattern A was slightly softer but again performed below knitting Pattern C between ON and OFF, as can be observed on the plot.

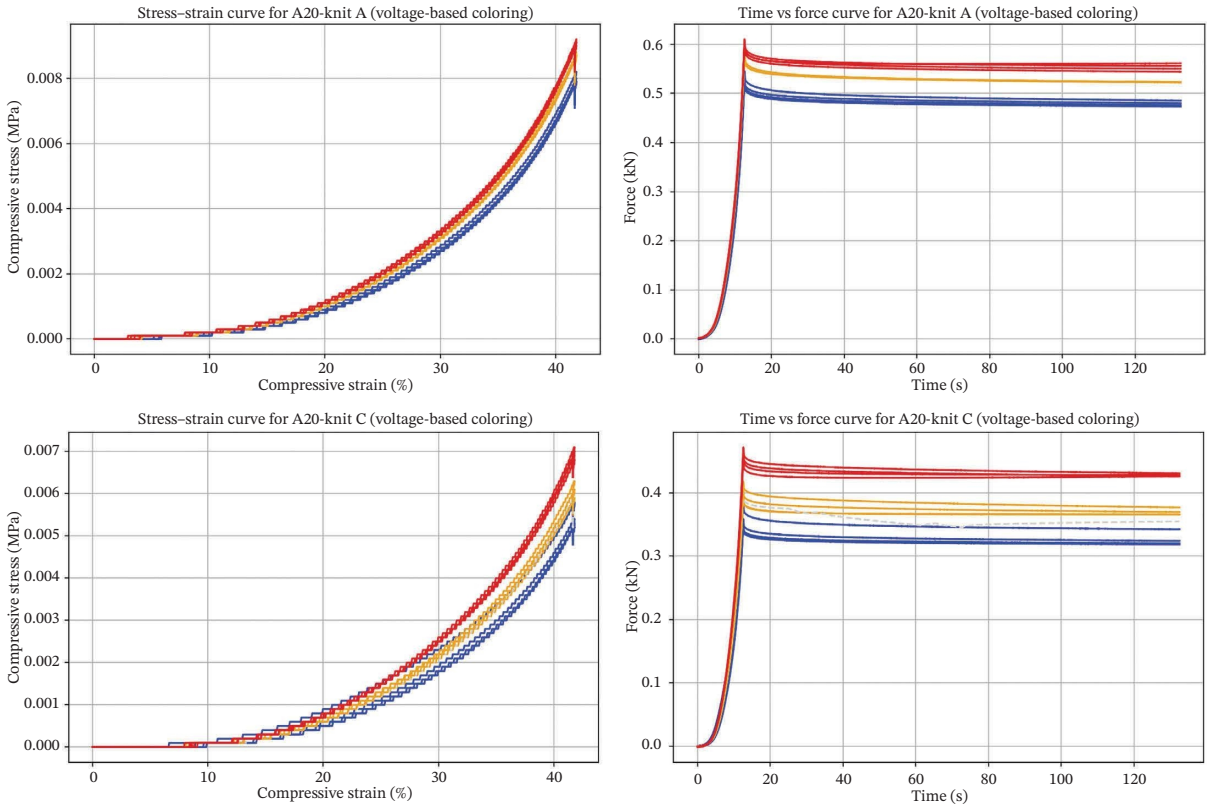

FIGURE 8 | Creep and relax test using the two substrates A20 on knitting patterns A and C; the first plot represents the strain (%) versus stress (MPa) and next to it a second plot of the time (s) versus force (kN), where the blue lines represent the material without voltage (OFF), the red lines represent the material with voltage (ON), and the gray lines represent faults in the test.

The analysis of compressive stress behavior across various materials and knit combinations of artificial muscles reveals notable findings regarding the responsiveness of these materials to external conditions such as voltage and temperature. The artificial muscle materials, particularly in combinations of A20 and A30 with different knit patterns, demonstrate a range of mechanical adaptability under compression, which is modulated by external stimuli like voltage. These variations imply that the artificial muscles can dynamically adjust their rigidity, becoming softer or harder in response to controlled changes in voltage or heat, an effect that could be highly beneficial in fields requiring adaptable mechanical properties.

For Material A20 with knit A, the stress–strain characteristics exhibit moderate variability, with a maximum compressive stress of 0.0092 MPa and a minimum of 0.0079 MPa, resulting in a 16.46% change in stress. This combination appears to provide a consistent compressive response with relatively minor fluctuations, indicating that it could maintain stable mechanical properties under minor voltage shifts. Conversely, material A20 with knit C shows a broader range of compressive responses, with a 36.54% change in stress, reflecting a higher sensitivity to external modulation; see Figure 8.

Material A30 with knit A demonstrates higher rigidity with a maximum compressive stress of 0.0122 MPa and a minimum of 0.0093 MPa, corresponding to a 31.18% change. This increased stress threshold indicates that the material can withstand higher compressive loads while allowing for moderate adaptability in response to changes in voltage or temperature. On the other hand, material A30 with knit C shows the highest stress variability, with a 35.71% change in stress. The large difference in the compressive response suggests that this combination may be ideal for applications requiring substantial mechanical adaptability while retaining the ability to transition between softer and stiffer states; see Figure 9.

The relationship between voltage and compressive stress across these artificial muscle combinations is significant, as higher voltages are associated with increased stress levels. This implies that voltage can serve as a reliable external control to modulate stiffness and softness, which could be leveraged in real-time applications where material compliance must be adjusted dynamically.

The differences between knit patterns also underscore the importance of structural design in achieving desired mechanical properties, with some combinations more responsive to voltage shifts than others.

5.3.1 | Implications

The results suggest that both the material type and the knitting pattern significantly affect the stress response under electrical actuation.

Specifically:

- Knitting Pattern C consistently outperforms Pattern A in both substrates (A20 and A30), demonstrating greater increases in stress when actuated.
- Substrate A30 shows a higher overall stress response compared to A20, indicating its superior performance in applications requiring higher compressive resistance.

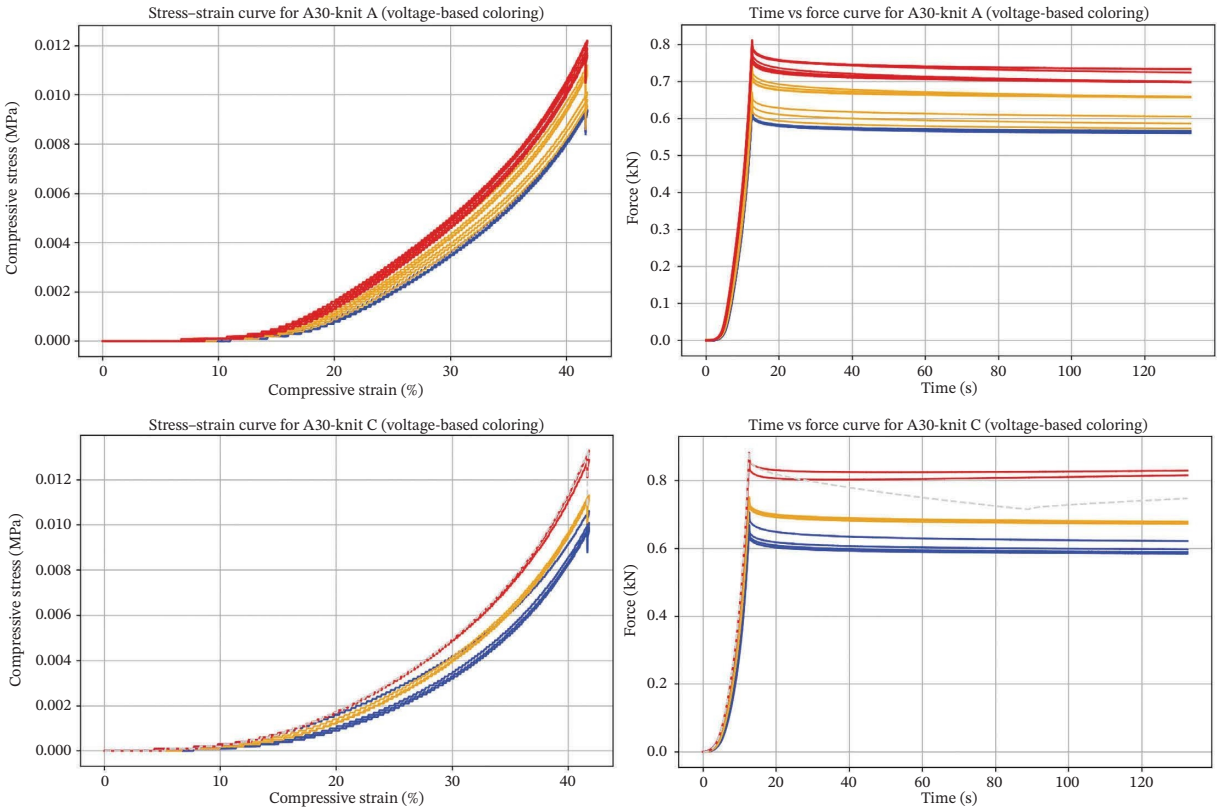

FIGURE 9 | Creep and relax test using the two substrates A30 on knitting patterns A and C; the first plot represents the strain (%) versus stress (MPa) and next to it a second plot of the time (s) versus force (kN), where the blue lines represent the material without voltage (OFF), the red lines represent the material with voltage (ON), and the gray lines represent faults in the test.

- Electrical actuation effectively enhances the compressive resistance of these silicone substrates, with the degree of enhancement varying depending on the knitting pattern and substrate type.

These findings are crucial for designing and optimizing materials for applications where enhanced stress resistance and dynamic performance are required, such as in adaptive structural components in robotics and engineering.

5.4 | Statistical Analysis

Finally, an independent samples *t*-test was conducted to compare the test scores of two different silicone substrates A20 and A30 on the creep and relax stress data, where the test variable is the stress from the compression and the grouping variable is the material composition A20 or A30.

5.4.1 | Descriptive Statistics

5.4.1.1 | Group A20

- Sample size (n) = 165750
- Mean (M) = 0.006248 MPa
- Standard Deviation (SD) = 0.0019706 MPa

5.4.1.2 | Group A30

- Sample size (n) = 198900
- Mean (M) = 0.009362 MPa
- Standard Deviation (SD) = 0.0025678 MPa

5.4.1.3 | Comparison of Stress Levels

- The mean stress level for substrate A30 (0.009362 MPa) is significantly higher than that for substrate A20 (0.006248 MPa).
- The standard deviation for A30 (0.0025678 MPa) is also higher than that for A20 (0.0019706 MPa), indicating that stress levels in A30 are more dispersed around the mean. This suggests that A30 exhibits less predictable performance under stress compared to A20.

An independent samples *t*-test to compare test scores in Group A20 and Group A30. There was a significance in test scores between Group A20 ($M = 0.006248$, SD = 0.0019706) and Group A30 ($M = 0.009362$, SD = 0.0025678); $t(-404.395) = 364648$, $p < 0.001$. The effect size was ($d = 0.0023155$). The results showed a significant difference in stress between the A20 and A30 silicone substrates, the A30 being the one that produced the higher stress levels with a mean difference of −0.0031142. When observing the independent sample effect size, it is possible to observe a large effect size; Cohen's $d = -1.345$ (with a 95% confidence interval of −1.352 to −1.338), Hedges' correction = −1.345 (with a 95% confidence interval of −1.352 to −1.338), and Glass's delta = −1.213 (with a 95% confidence interval of −1.220 to −1.205),

which shows the substantial difference between A20 and A30 silicone substrates.

5.4.2 | Independent Samples *t*-Test

The *t*-test revealed a significant difference in stress levels between Group A20 and Group A30.

- Group A20 ($M = 0.006248$, SD = 0.0019706)
- Group A30 ($M = 0.009362$, SD = 0.0025678)
- t (-404.395) = 364648, $p < 0.001$

The mean difference in stress levels between A20 and A30 is −0.0031142 MPa, with A30 showing higher stress levels.

5.4.3 | Effect Size

5.4.3.1 | Cohen's *d*

- $d = -1.345$ (with a 95% confidence interval of −1.352 to −1.338)

5.4.3.2 | Hedges' Correction

- Hedges' correction = −1.345 (with a 95% confidence interval of −1.352 to −1.338)

5.4.3.3 | Glass's Delta

- Glass's delta = −1.213 (with a 95% confidence interval of −1.220 to −1.205).

These effect sizes indicate a large and substantial difference in stress levels between the A20 and A30 silicone substrates, with A30 exhibiting significantly higher stress.

5.4.4 | Implications

The results from the independent samples *t*-test and the accompanying descriptive statistics provide important insights:

- Higher stress levels in A30: Substrate A30 consistently shows higher stress levels under the same conditions compared to A20. This makes A30 more suitable for applications where higher stress tolerance is needed.
- Increased variability in A30: The higher standard deviation in A30 indicates more variability in its stress response, suggesting that while it can withstand higher stress, its performance is less predictable compared to A20. This could be a consideration in applications where consistency and reliability are critical.
- Significant difference and large effect size: The significant *t*-test results and large effect size measures (Cohen's *d*, Hedges' correction, and Glass's delta) confirm that the difference in stress levels between A20 and A30 is not only statistically significant but also practically meaningful.

In conclusion, the independent samples *t*-test analysis demonstrates that the A30 silicone substrate exhibits significantly higher stress levels than A20, albeit with greater variability. This indicates that A30 may be preferred in applications requiring higher stress tolerance, but the variability should be considered when consistency is essential. The substantial effect size further underscores the importance of these findings for material selection and application design in engineering and manufacturing contexts.

5.4.5 | Effect Size Discrepancy

The reported effect size ($d = 0.0023155$) is very small, suggesting that despite the significant p value, the practical difference between the two groups might be minimal. This small effect size indicates that, while A30 exhibits higher stress levels, the magnitude of this difference in practical terms is not substantial.

In contrast, the other effect size measures (Cohen's *d*, Hedges' correction, and Glass's delta) indicate large effect sizes (around −1.345), which are contradictory to the initially reported small effect size.

The independent samples *t*-test shows a statistically significant difference in stress levels between A20 and A30 silicone substrates, with A30 exhibiting higher stress levels.

However, the interpretation of the effect size presents a complex picture:

- Small effect size ($d = 0.0023155$): Suggests minimal practical difference, highlighting the need for context-specific evaluation.
- Large effect sizes (around −1.345): Indicates substantial practical importance, especially for high stress applications.

Overall, while A30 demonstrates higher stress levels and thus potential for higher performance in demanding applications, its greater variability and the mixed implications of effect size warrant careful consideration in material selection and application design.

5.5 | Footwear Comparison

Subsequently, we compared our results with the current running footwear from the market [raw Force data in Newtons].

The dataset we are analyzing contains only force-related data, using different brands and models of the market, by compression the heel part of the shoe and our prototype under a uniform displacement of 12.5 mm. This assumption allows us to use the force data (FmaxN) to infer how each model behaves under this fixed displacement.

5.5.1 | Force–Displacement Relationship

Since each model experienced the same 12.5 mm displacement, we can interpret the recorded force values as indicative of the rigidity or stiffness. In a real-world scenario, stiffness K is defined as follows:

$$k = \frac{F}{\Delta x}, \tag{1}$$

where F is the force and Δx is the displacement. Since Δx is constant (12.5 mm), the force values directly reflect the stiffness: the higher the force, the more rigid the material. Then, we compared the mean force values (in Newtons) for different brands and models to infer their relative rigidity under the same 12.5 mm displacement.

Data from the compression tests show that the On Cloudflyer 4 was the hardest material on the heel, followed by the Adidas Ultraboost, Nike Zoom Fly 5, Adidas Adizero Adios Pro 3, and the Hoka Bondi X, while the Nike Air Zoom Tempo Next% was the softest material in the heel. It is important to consider that the Nike Air Zoom Tempo Next% is an ultra-responsive type of running footwear with higher than average energy return when compressed, and this is the reason why marathon professional runners tend to use this supper responsive cushioning systems, and several brands have options with these capabilities; see Figure 4.

When comparing our smart composite with footwear from the market, it is possible to observe the different ranges in compressive stress of the smart composite when it is OFF and actuated in the three silicones tested (A12, A20, and A30).

We can observe that the A30 substrate with the knitting Pattern A ranged between 740.3 N (OFF) and 885.5 N (ON), with a maximum difference of 145.2 N. In comparison, the A30 substrate with the knitting Pattern C had a range between 803.3 N (OFF) and 1029.4 N (ON), with a maximum difference of 226.1 N. On the other hand, the substrate A20 with the knitting Pattern A exhibited a stress of 610.7 N (OFF) and 662.6 N (ON) with a maximum difference of 51.9 N; meanwhile, the A20 with a knitting Pattern C had 410.9 N (OFF) and 569 N (ON) with a maximum difference of 158.1 N. Finally, the substrate A12 with the knitting Pattern A achieved 317.7 N (OFF) and 399.3 N (ON) with a maximum difference of 81.6 N, and A12 with the knitting Pattern C showed 239.4 N (OFF) and 327.9 N (ON) with a maximum difference of 88.5 N; see Figure 4.

Also, when comparing the results from our compression tests with the current running footwear, we can observe that we have developed a range that covers different cushioning types. For example, the Adidas Adizero Adios Pro 3 (which is an exceptionally soft shoe for running) reached around 380 N, while the Adidas Switch FWD did around 420 N. This range difference in softness cushioning can be covered by our artificial muscle A12 with the knitting Pattern A, which can change from 317 N (OFF) to 400 N (ON). In comparison, the prototype A20 knit C exhibited between 410 N (OFF) and 569 N (ON) and covered an extensive range of harder sole footwear for running, allowing us to cover the whole range of cushioning just using 2 samples.

The following interpretation highlights the key findings.

5.5.2 | Comparison With Running Footwear

- Hardest heel material: The On Cloudflyer 4 was identified as having the hardest heel material, followed by Adidas Ultraboost, Nike Zoom Fly 5, Adidas Adizero Adios Pro 3, and Hoka Bondi X. The Nike Air Zoom Tempo Next% was the softest material in the heel.
- Softest heel material: The Nike Air Zoom Tempo Next% is noted for its ultra-responsiveness and high energy return, which is preferred by marathon runners for its cushioning system.

5.5.3 | Impact of Cushioning

- Higher cushioning reduces impact on the heel, providing more comfort while running. This type of cushioning is favored for longer races.
- Harder soles produce more responsive and faster running, which might be preferred for shorter, more intense runs.

5.5.4 | Performance of Silicone Substrates

5.5.4.1 | A30 Substrate

- Knitting Pattern A: Range between 740.3 N (OFF) and 885.5 N (ON) with a maximum difference of 145.2 N.
- Knitting Pattern C: Range between 803.3 N (OFF) and 1029.4 N (ON) with a maximum difference of 226.1 N.

5.5.4.2 | A20 Substrate

- Knitting Pattern A: Range between 610.7 N (OFF) and 662.6 N (ON) with a maximum difference of 51.9 N.
- Knitting Pattern C: Range between 410.9 N (OFF) and 569 N (ON) with a maximum difference of 158.1 N.

5.5.4.3 | A12 Substrate

- Knitting Pattern A: Range between 317.7 N (OFF) and 399.3 N (ON) with a maximum difference of 81.6 N.
- Knitting Pattern C: Range between 239.4 N (OFF) and 327.9 N (ON) with a maximum difference of 88.5 N.

5.5.4.4 | Comparison With Specific Running Shoes

- The artificial muscle A12 with knitting Pattern A can range from 317 N (OFF) to 400 N (ON), covering the range of softer cushioning found in some running shoes.
- The prototype A20 with knitting Pattern C covers a range between 410 N (OFF) and 569 N (ON), aligning with harder sole footwear for running.

5.5.4.5 | General Range of Running Footwear. The running footwear tested had a force range between 349 N and 497 N, which the tested silicone substrates can encompass with their respective knitting patterns and actuation states.

The results show that the smart composites (A12, A20, A30) developed can effectively mimic and even exceed the performance characteristics of the current running footwear in terms of compressive force and cushioning. The ability of these materials to adjust their compressive force when actuated (ON) demonstrates their potential for application in adaptive footwear technologies.

6 | Discussion

The findings from the comprehensive analysis of the smart composite materials reveal several important insights into their mechanical performance and potential applications.

This study investigated how silicone substrate hardness, SMA actuation state, and knitting pattern collectively influence the mechanical behavior of a smart composite intended for adaptive footwear applications.

Three consistent findings emerged across the compression and creep–relax experiments.

Data showed that these embedding systems (knitting patterns) enable smart composites to be tuned to achieve different levels of rigidity and compliance, which is advantageous for adaptive applications. A MANOVA confirms that material hardness and actuation state are the primary factors influencing mechanical performance, while interactions are less dominant but still relevant. Notably, the actuation–material interaction suggests that responsiveness can be tailored by combining substrate hardness with electrical activation. Post hoc tests (Tukey HSD and Bonferroni) also showed significant mean differences across materials for all variables, reinforcing the distinct behavior of each silicone substrate under stress.

The magnitude of actuation effects varied with substrate hardness. As expected from elastomer mechanics, the harder A30 silicone generated the highest absolute stress values, whereas A12 produced the lowest. Softer substrates dissipated deformation more efficiently, reducing the effective translation of SMA contraction into bulk stress.

Results demonstrated that knitting Pattern C produced substantially greater differences between ON and OFF conditions than Pattern A across all substrates, especially when combined with silicone shore A30, which yields higher adaptability and stress response, suggesting enhanced efficiency in stress distribution and elasticity. This enhanced responsiveness appears to be driven by the symmetric, dual-direction arrangement of SMA routing in knitting Pattern C, which enables more efficient load transfer and coordinated deformation across the multicell architecture. In contrast, knitting Pattern A unidirectional layout constrained deformation along a more limited axis, resulting in lower actuation-induced stiffness changes. These findings highlight the importance of substrate selection in achieving a desired stiffness range.

Creep and relax tests further confirmed these findings, showing that the A30 material had the highest stress and greater variability than the A20 material. This ability to dynamically adjust stiffness could be beneficial for wearable applications, such as footwear, where adaptability to different movement patterns and shock absorption is crucial. These insights align with the *t*-test results, which confirmed results, indicating a substantial difference in compressive performance between the two materials. This statistical result aligns with the mechanical findings, confirming that substrate A30 offers higher rigidity and stress resistance, making it a better choice for applications requiring high compressive strength.

When analyzing the differences between running footwear from the market and our artificial muscle, across the three substrates, the smart composites exhibited a force range of approximately 239 N–1030 N under a standard compressive displacement of 12.5 mm. This range overlaps with the stiffness characteristics of commercial running footwear tested for comparison, including soft high-energy-return models and firmer stability shoes. Importantly, the shift between soft and firm states can be achieved through activation of a single composite, whereas commercial midsoles provide only a fixed mechanical response.

This overlap suggests that the proposed artificial muscle midsole system has the potential to replace multiple traditional cushioning types with a single configurable material, offering dynamic stiffness profiles that could improve performance, comfort, and injury risk mitigation.

In the context of variable elasticity, the porosity and internal cellular arrangement of the composite play a critical role in determining its mechanical adaptability. Similar to biological muscle, which exhibits a hierarchical porous structure consisting of aligned fibers, sarcomere gaps, and extracellular matrix channels, the present artificial muscle composite uses interconnected silicone tubing to replicate a functionally graded architecture. This controlled porosity enables localized deformation, stress redistribution, and energy dissipation under compression, closely mimicking the viscoelastic behavior of muscle tissue. When SMA wires contract, this porosity is selectively reduced or reoriented, producing changes in local density and effective stiffness analogous to muscle fiber recruitment during contraction, such as the metamaterials' porosity-controlled response to the intrinsic adaptability of biological muscle. Knitting Pattern C enhances this effect by enabling a more uniform deformation of the porous network, functioning similarly to how muscle architecture coordinates deformation across fascicle bundles. Therefore, the artificial muscle not only reproduces the mechanical transition observed in living tissues from the relaxed to the contracted phase but also provides an engineered pathway to control stiffness through geometric and porosity designs.

The ability to dynamically adjust mechanical properties provides a versatile and customizable solution for enhancing performance, fit, balance control, pressure distribution, and comfort.

Future research should focus on validating the long-term performance of these materials, exploring advanced applications, and integrating emerging technologies to unlock their full potential. Further studies should also incorporate ergonomic testing with human participants and multicycle fatigue analyses to confirm that the composite behaves consistently under diverse locomotor conditions. Addressing these factors will be essential to establishing the composite's suitability for real-world applications and ensuring that its adaptive capabilities translate to meaningful improvements in comfort, performance, and user safety. Through interdisciplinary collaboration and innovative research, smart composites can revolutionize multiple industries and improve the quality of life for users.

7 | Conclusion

The aim of this study was to evaluate how silicone substrate hardness, SMA actuation state, and knitting pattern influence the stiffness, adaptability, and compressive behavior of an artificial muscle intended for adaptive footwear applications. The results from the compression and creep–relax experiments provide clear evidence that each factor plays a significant role in shaping the composite's mechanical response, directly supporting the stated aim.

We investigated the current techniques for the development of a novel smart composite with muscle behavior, capable of dynamically changing its flexibility and elasticity with applications in footwear technology, while highlighting its importance in balance and muscle control during movement. Current technology in metamaterials provides the foundations for the development of an artificial muscle capable of upholding the forces

and stress in an affordable, long-lasting, and reliable smart system with multifunctional capabilities.

We have presented two different embedding techniques using smart materials to control the deformation behavior of a flexible substrate structure made of fibers that can control the muscle behavior when compressed. The embedding technique described in this study is called knitting patterns, as it generates a series of interlocking mechanisms that can dynamically compress and relax the structure while in use.

Both knitting patterns presented in this paper were tested during compression in both states: ON and OFF. The study provides compelling evidence that the type of material utilized to support the substrate and the knitting pattern used significantly influences the stress response and elasticity of the material during compression testing. Where the silicone material A30 shore, in combination with the knitting Pattern C, consistently exhibited the highest stress differences among all combinations, making it the best candidate for applications requiring high elasticity, such as artificial muscles, soft robotics for the development of stimuli-responsive devices for walking assisting in rehabilitation to improve muscle control. Lastly, significant main effects and interactions were found with the MANOVA and comprehensive post hoc analyses, underscoring the importance of considering both material composition (A20 and A30) and structural design in developing advanced materials with bespoke mechanical properties. Future research should explore long-term performance and durability of these materials under repeated stress cycles to further validate their applicability in practical scenarios.

Results show that both knitting patterns behave differently during compression, which allows us to compare them with various types of footwear from the industry. These differences generate a vast amount of possibility in terms of the needs for actuation depending on the activity required during movement, which is supported by the comparative analysis with running footwear from the market, demonstrating the potential applications of this artificial muscle and knitting patterns, providing customizable cushioning and support capabilities.

This study demonstrated that embedding SMAs into silicone substrates using specific knitting patterns enables dynamic modulation of mechanical properties in footwear midsoles. Among the tested configurations, knitting Pattern C combined with silicone A30 consistently exhibited the highest stress response under actuation, with up to a 36.54% increase in compressive stress during creep and relaxation. These findings confirm the effectiveness of electrical actuation in tuning midsole stiffness and elasticity, opening the door to customizable footwear systems tailored to user needs. This adaptable material behavior has potential applications in athletic performance, injury prevention, and rehabilitation. Future research will focus on long-term durability and real-world usage to validate sustained performance.

Acknowledgments

The authors would like to thank the UCL Cardiovascular Engineering Laboratory and the Materials Laboratory at University College London in Mechanical engineering, Roberts Engineering Building, University College London, Torrington Place, London WC1E 7JE, for allowing them to perform their tests. The authors also acknowledge research assistant Hilda Diaz for her contributions to the development, data collection, processing, and analysis. This study did not receive external funding and was fully self-funded. Patent pending GB2309346.1.

Funding

This study did not receive external funding.

Conflicts of Interest

The authors declare no conflicts of interest.

Data Availability Statement

The data that support the findings of this study are available from the corresponding author upon reasonable request.

References

1. A. Davis, T. Haines, and C. Williams, "Do Footwear Styles Cause Falls or Increase Falls Risk in Healthy Older Adults? A Systematic Review," *Footwear Science* 11, no. 1 (2019): 13–23, https://doi.org/10.1080/19424280.2018.1555861.

2. C. J. Barton, D. Bonanno, and H. B. Menz, "Development and Evaluation of a Tool for the Assessment of Footwear Characteristics," *Journal of Foot and Ankle Research* 2, no. 1 (2009): 10, https://doi.org/10.1186/1757-1146-2-10.

3. H. Reimann, T. Fettrow, E. D. Thompson, and J. J. Jeka, "Neural Control of Balance During Walking," *Frontiers in Physiology* 9 (2018): 1271, https://doi.org/10.3389/fphys.2018.01271.

4. F. B. Horak and L. M. Nashner, "Central Programming of Postural Movements: Adaptation to Altered Support-Surface Configurations," *Journal of Neurophysiology* 55, no. 6 (1986): 1369–1381, https://doi.org/10.1152/jn.1986.55.6.1369.

5. A. L. Hof and J. Duysens, "Responses of Human Ankle Muscles to Mediolateral Balance Perturbations During Walking," *Human Movement Science* 57 (2018): 69–82, https://doi.org/10.1016/j.humov.2017.11.009.

6. J. Tavares, T. Jost, G. Drewelow, and J. Rylander, "Do Maximalist Shoes Mitigate Risk Factors for Tibial Stress Fractures Better Than Stability or Flexible (Marketed as Minimalist) Shoes?" *Footwear Science* 12, no. 1 (2020): 63–74, https://doi.org/10.1080/19424280.2019.1708977.

7. C. E. Milner, I. S. Davis, and J. Hamill, "Free Moment as a Predictor of Tibial Stress Fracture in Distance Runners," *Journal of Biomechanics* 39, no. 15 (2006): 2819–2825, https://doi.org/10.1016/j.jbiomech.2005.09.022.

8. R. J. Butler, I. S. Davis, and J. Hamill, "Interaction of Arch Type and Footwear on Running Mechanics," *The American Journal of Sports Medicine* 34, no. 12 (2006): 1998–2005, https://doi.org/10.1177/0363546506290401.

9. E. Day and M. Hahn, "Optimal Footwear Longitudinal Bending Stiffness to Improve Running Economy Is Speed Dependent," *Footwear Science* 12, no. 1 (2020): 3–13, https://doi.org/10.1080/19424280.2019.1696897.

10. M. R. Shorten, "The Energetics of Running and Running Shoes," *Journal of Biomechanics* 26 (1993): 41–51, https://doi.org/10.1016/0021-9290(93)90078-s.

11. H. Kinoshita and B. T. Bates, "The Effect of Environmental Temperature on the Properties of Running Shoes," *Journal of Applied Biomechanics* 12, no. 2 (1996): 258–268, https://doi.org/10.1123/jab.12.2.258.

12. L. Wang, J. Xian Li, Y. Hong, and J. He Zhou, "Changes in Heel Cushioning Characteristics of Running Shoes With Running Mileage. Footwear Science," *Footwear Science* 2, no. 3 (2010): 141–147, https://doi.org/10.1080/19424280.2010.519348.

13. J. Huang, "Effects of the Material of Running Shoes on Biomechanical Characteristics During Running," *Mechanics of Advanced*

Materials and Structures 26, no. 24 (2019): 2017–2022, https://doi.org/10.1080/15376494.2018.1513613.

14. L. Ferris, N. A. Sharkey, T. S. Smith, and D. K. Matthews, "Influence of Extrinsic Plantar Flexors on Forefoot Loading During Heel Rise," *Foot & Ankle International* 16, no. 8 (1995): 464–473, https://doi.org/10.1177/107110079501600802.

15. H. DeBusk, C. M. Hill, H. Chander, A. C. Knight, and K. Babski-Reeves, "Influence of Military Workload and Footwear on Static and Dynamic Balance Performance," *International Journal of Industrial Ergonomics* 64 (2018): 51–58, https://doi.org/10.1016/j.ergon.2017.11.003.

16. A. Simkin, I. Leichter, M. Giladi, M. Stein, and C. Milgrom, "Combined Effect of Foot Arch Structure and an Orthotic Device on Stress Fractures," *Foot & Ankle* 10, no. 1 (1989): 25–29, https://doi.org/10.1177/107110078901000105.

17. C. M. Hill, H. DeBusk, A. C. Knight, and H. Chander, "Influence of Military-Type Workload and Footwear on Muscle Exertion During Static Standing," *Footwear Science* 9, no. 3 (2017): 169–180, https://doi.org/10.1080/19424280.2017.1403968.

18. N. Forestier and P. Toschi, "The Effects of an Ankle Destabilization Device on Muscular Activity While Walking," *International Journal of Sports Medicine* 26, no. 6 (2005): 464–470, https://doi.org/10.1055/s-2004-830336.

19. L. Donovan, J. M. Hart, and J. Hertel, "Effects of 2 Ankle Destabilization Devices on Electromyography Measures During Functional Exercises in Individuals With Chronic Ankle Instability," *Journal of Orthopaedic & Sports Physical Therapy* 45, no. 3 (2015): 220–232, https://doi.org/10.2519/jospt.2015.5222.

20. E. Eils, S. Nolte, M. Tewes, L. Thorwesten, K. Völker, and D. Rosenbaum, "Modified Pressure Distribution Patterns in Walking Following Reduction of Plantar Sensation," *Journal of Biomechanics* 35, no. 10 (2002): 1307–1313, https://doi.org/10.1016/s0021-9290(02)00168-9.

21. K. Song, T. K. Kang, E. A. Wikstrom, H. Jun, and S. Y. Lee, "Effects of Reduced Plantar Cutaneous Sensation on Static Postural Control in Individuals With and Without Chronic Ankle Instability," *Journal of Science and Medicine in Sport* 20, no. 10 (2017): 910–914, https://doi.org/10.1016/j.jsams.2016.04.011.

22. E. M. Day and M. E. Hahn, "Does Running Speed Affect the Response of Joint Level Mechanics in Non-Rearfoot Strike Runners to Footwear of Varying Longitudinal Bending Stiffness?" *Gait & Posture* 84 (2021): 187–191, https://doi.org/10.1016/j.gaitpost.2020.11.029.

23. D. J. Stefanyshyn and J. W. Wannop, "The Influence of Forefoot Bending Stiffness of Footwear on Athletic Injury and Performance," *Footwear Science* 8, no. 2 (2016): 51–63, https://doi.org/10.1080/19424280.2016.1144652.

24. T. O. Clanton and J. J. Ford, "Turf Toe Injury," *Clinics in Sports Medicine* 13, no. 4 (1994): 731–741, https://doi.org/10.1016/s0278-5919(20)30282-9.

25. J. J. McCormick and R. B. Anderson, "Turf Toe: Anatomy, Diagnosis, and Treatment," *Sport Health* 2, no. 6 (2010): 487–494, https://doi.org/10.1177/1941738110386681.

26. J. Crandall, E. C. Frederick, R. Kent, D. J. Lessley, and C. Sherwood, "Forefoot Bending Stiffness of Cleated American Football Shoes," *Footwear Science* 7, no. 3 (2015): 139–148, https://doi.org/10.1080/19424280.2015.1058427.

27. R. T. Hockenbury, "Forefoot Problems in Athletes," *Medicine & Science in Sports & Exercise* 31, no. 7 Suppl (1999): S448–S458, https://doi.org/10.1097/00005768-199907001-00006.

28. J. P. R. Roy and D. J. Stefanyshyn, "Shoe Midsole Longitudinal Bending Stiffness and Running Economy, Joint Energy, and EMG," *Medicine & Science in Sports & Exercise* 38, no. 3 (2006): 562–569, https://doi.org/10.1249/01.mss.0000193562.22001.e8.

29. D. Stefanyshyn and C. Fusco, "Athletics: Increased Shoe Bending Stiffness Increases Sprint Performance," *Sports Biomechanics* 3, no. 1 (2004): 55–66, https://doi.org/10.1080/14763140408522830.

30. N. Tinoco, D. Bourgit, and J. B. Morin, "Influence of Midsole Metatarsophalangeal Stiffness on Jumping and Cutting Movement Abilities," *Proceedings of the Institution of Mechanical Engineers – Part P: Journal of Sports Engineering and Technology* 224, no. 3 (2010): 209–217, https://doi.org/10.1243/17543371jset69.

31. A. Arndt, P. Westblad, I. Ekenman, and A. Lundberg, "A Comparison of External Plantar Loading and *In Vivo* Local Metatarsal Deformation Wearing Two Different Military Boots," *Gait & Posture* 18, no. 2 (2003): 20–26, https://doi.org/10.1016/s0966-6362(02)00191-1.

32. J. Paulose, A. S. Meeussen, and V. Vitelli, "Selective Buckling via States of Self-Stress in Topological Metamaterials," *Proceedings of the National Academy of Sciences* 112, no. 25 (2015): 7639–7644, https://doi.org/10.1073/pnas.1502939112.

33. A. A. Zadpoor, "Mechanical Meta-Materials," *Materials Horizons* 3, no. 5 (2016): 371–381, https://doi.org/10.1039/c6mh00065g.

34. S. Sărăndan, R. Negru, L. Marşavina, and D. A. Şerban, "Cellular Materials Used in Athletic Footwear Applications: Experimental, Analytical and Numerical Investigations," *Materials Today: Proceedings* 45 (2021): 4310–4314, https://doi.org/10.1016/j.matpr.2020.12.796.

35. D. J. N. Amorim, T. Nachtigall, and M. B. Alonso, "Exploring Mechanical Meta-Material Structures Through Personalised Shoe Sole Design," in *Proceedings of the 2019 ACM Symposium on Computational Fabrication* (Pittsburgh, PA: ACM, 2019).

36. Y. F. Hudak, J. S. Li, S. Cullum, et al., "A Novel Workflow to Fabricate a Patient-Specific 3D Printed Accommodative Foot Orthosis With Personalized Latticed Metamaterial," *Medical Engineering & Physics* 104 (2022): 103802, https://doi.org/10.1016/j.medengphy.2022.103802.

37. S. Gao, A. K. Gain, and L. Zhang, "A Metamaterial for Wearable Piezoelectric Energy Harvester," *Smart Materials and Structures* 30, no. 1 (2020): 015026, https://doi.org/10.1088/1361-665x/abca09.

38. A. Ion, J. Frohnhofen, L. Wall, et al., "Metamaterial Mechanisms," in *Proceedings of the 29th Annual Symposium on User Interface Software and Technology* (Tokyo, 2016), 529–539, https://doi.org/10.1145/2984511.2984540.

39. L. Lu, A. Sharf, H. Zhao, et al., "Build-to-Last: Strength to Weight 3D Printed Objects," *ACM Transactions on Graphics* 33, no. 4 (2014): 1–10, https://doi.org/10.1145/2601097.2601168.

40. W. Wang, Y. J. Liu, J. Wu, et al., "Support-Free Hollowing," *IEEE Transactions on Visualization and Computer Graphics* 24, no. 10 (2017): 2787–2798, https://doi.org/10.1109/tvcg.2017.2764462.

41. R. Prévost, E. Whiting, S. Lefebvre, and O. Sorkine-Hornung, "Make It Stand: Balancing Shapes for 3D Fabrication," *ACM Transactions on Graphics* 32, no. 4 (July 2013): 1–10, https://doi.org/10.1145/2461912.2461957.

42. J. Wang, J. Callanan, O. Ogunbodede, and R. Rai, "Hierarchical Combinatorial Design and Optimization of Non-Periodic Metamaterial Structures," *Additive Manufacturing* 37 (2021): 101710, https://doi.org/10.1016/j.addma.2020.101710.

43. S. Felton, M. Tolley, E. Demaine, D. Rus, and R. Wood, "A Method for Building Self-Folding Machines," *Science.* 345, no. 6197 (2014): 644–646, https://doi.org/10.1126/science.1252610.

44. L. Seigner, G. K. Tshikwand, F. Wendler, and M. Kohl, "Bi-Directional Origami-Inspired SMA Folding Microactuator," in *Actuators [Internet]* (Basel: MDPI, 2021), 181.

45. C. Lv, D. Krishnaraju, G. Konjevod, H. Yu, and H. Jiang, "Origami Based Mechanical Metamaterials," *Scientific Reports* 4, no. 1 (2014): 5979, https://doi.org/10.1038/srep05979.

46. J. L. Silverberg, A. A. Evans, L. McLeod, et al., "Using Origami Design Principles to Fold Reprogrammable Mechanical Metamaterials," *Science* 345, no. 6197 (2014): 647–650, https://doi.org/10.1126/science.1252876.

47. K. Kuribayashi, K. Tsuchiya, Z. You, et al., "Self-Deployable Origami Stent Grafts as a Biomedical Application of Ni-Rich TiNi Shape Memory Alloy Foil," *Materials Science and Engineering A* 419, no. 1-2 (2006): 131–137, https://doi.org/10.1016/j.msea.2005.12.016.

48. D. Stoeckel, "Nitinol Medical Devices and Implants," *Minimally Invasive Therapy & Allied Technologies* 9, no. 2 (2000): 81–88, https://doi.org/10.3109/13645700009063054.

49. W. Van Moorleghem, M. Chandrasekaran, D. Reynaerts, J. Peirs, and H. Van Brussel, "Shape Memory and Superelastic Alloys: The New Medical Materials With Growing Demand," *Bio-Medical Materials and Engineering* 8, no. 2 (1998): 55–60.

50. J. Ryhänen, "Biocompatibility Evaluation of Nickel-Titanium Shape Memory Metal Alloy," (1999), https://oulurepo.oulu.fi/handle/10024/36985.

51. R. Pelrine, J. Eckerle, and S. Chiba, "Review of Artificial Muscle Approaches," in *Proceedings of the 3rd International Symposium on Micro Machine and Human Science* (Nagoya, 1992).

52. S. M. Mirvakili and I. W. Hunter, "Artificial Muscles: Mechanisms, Applications, and Challenges," *Advanced Materials* 30, no. 6 (2018): 1704407, https://doi.org/10.1002/adma.201704407.

53. S. M. Mirvakili, A. Pazukha, W. Sikkema, et al., "Niobium Nanowire Yarns and Their Application as Artificial Muscles," *Advanced Functional Materials* 23, no. 35 (2013): 4311–4316, https://doi.org/10.1002/adfm.201203808.

54. J. W. Wannop, A. Killick, R. Madden, and D. J. Stefanyshyn, "The Influence of Gearing Footwear on Running Biomechanics," *Footwear Science* 9, no. 2 (May 2017): 111–119, https://doi.org/10.1080/19424280.2017.1342705.

55. J. C. Erhart, C. O. Dyrby, D. D. D'Lima, C. W. Colwell, and T. P. Andriacchi, "Changes in *In Vivo* Knee Loading With a Variable-Stiffness Intervention Shoe Correlate With Changes in the Knee Adduction Moment," *Journal of Orthopaedic Research* 28, no. 12 (2010): 1548–1553, https://doi.org/10.1002/jor.21183.

56. N. Moslemi, S. Gohari, F. Mozafari, et al., "A Novel Smart Assistive Knee Brace Incorporated With Shape Memory Alloy Wire Actuator," *Journal of Intelligent Material Systems and Structures* 31, no. 13 (2020): 1543–1556, https://doi.org/10.1177/1045389x20922911.

57. E. T. Esfahani and M. H. Elahinia, "Stable Walking Pattern for an SMA-Actuated Biped," *IEEE* 12, no. 5 (2007): 534–541, https://doi.org/10.1109/tmech.2007.905707.

58. K. Y. Tu, T. T. Lee, C. H. Wang, and C. A. Chang, "Design of a Fuzzy Walking Pattern (FWP) for a Shape Memory Alloy (SMA) Biped Robot," *Robotica* 17, no. 4 (1999): 373–382, https://doi.org/10.1017/s0263574799001617.

59. A. Alminnawi, Y. Kobayashi, T. Otani, and M. Tanaka, "Shape Memory Alloy Actuated Ankle Foot Orthosis for Reduction of Locomotion Force," in *Proceedings of the 2021 World Automation Congress (WAC)* (Taipei, 2021).

60. C. Lecomte, A. L. Ármannsdóttir, F. Starker, H. Tryggvason, K. Briem, and S. Brynjolfsson, "Variable Stiffness Foot Design and Validation," *Journal of Biomechanics* 122 (2021): 110440, https://doi.org/10.1016/j.jbiomech.2021.110440.

61. W. M. Chen, Y. Yu, X. Geng, C. Wang, L. Chen, and X. Ma, "Modulation of Internal Tissue Stresses of the Knee via Control of Variable-Stiffness Properties in a 3D-Printed Footwear: A Combined Experimental and Finite Element Analysis," *Medical Engineering & Physics* 104 (2022): 103800, https://doi.org/10.1016/j.medengphy.2022.103800.

62. K. Baousi, N. Fear, C. Mourouzis, et al., "Inflashoe: A Shape Changing Shoe to Control Underfoot Pressure," in *Proceedings of the 2017 CHI Conference Extended Abstracts on Human Factors in Computing Systems* (Denver, CO, 2017), 2381–2387, https://doi.org/10.1145/3027063.3053190.

63. B. Mosadegh, P. Polygerinos, C. Keplinger, et al., "Pneumatic Networks for Soft Robotics That Actuate Rapidly," *Advanced Functional Materials* 24, no. 15 (2014): 2163–2170, https://doi.org/10.1002/adfm.201303288.

64. M. Sasagawa, A. Niijima, K. Eguchi, et al., "Lower Limb Muscle Activity Control by Using Jamming Footwear," in *Proceedings of the 2019 41st Annual International Conference of the IEEE Engineering in Medicine and Biology Society (EMBC)* (Berlin: IEEE, 2019), 3302–3305.

65. Dynalloy, *FLEXINOL® Actuator Wires* (Dynamic Alloys, 2023), https://www.dynalloy.com/flexinol.php.

66. Dynalloy Inc, "Makers of Dynamic Alloys," (2023), https://www.dynalloy.com/tech_data_wire.php.